Electronic Supplementary Material (ESI) for New Journal of Chemistry.

Electronic Supplementary Information

Activating Bimetallic ZIF-derived Polymers Using Facile Steam-Etching for ORR

Yanling Wu [a], Miantuo Li [b], Liping Ma [a], Minghui Lu [a], Haijun Zhang [c,*], Meili Qi [a,*]

a. *School of Transportation and Civil Engineering, Shandong Jiaotong University, Ji'nan 250357, China. E-mail: beauty0507@163.com.*

b. *School of Materials Science and Engineering, China University of Petroleum (East China), Qingdao 266580, China.*

c. *Department of Vascular & Intervention, Tenth Peoples' Hospital of Tongji University, Shanghai 200072, China. E-mail:zhanghaijun@tongji.edu.cn.*

The experiment section

1. Chemical and reagents

Zinc nitrate ($Zn(NO_3)_2·6H_2O$), ferric nitrate hexahydrate ($Fe(NO_3)_3·9H_2O$), N, N'-carbonyldiimidazole (CDI), dicyandiamide (DICY), PEG 2000, and phytic acid (PA) were purchased from Aladdin (Shanghai, China). Nafion (5 wt.%) and commercial platinum/carbon (20 wt.% Pt/C) were purchased from Alfa Aesar Co. Ltd.

2. Preparation process of precursor 1

Initially, 40 mmol CDI was dissolved into 100 mL ethanol and 10 mmol $Zn(NO_3)_2·6H_2O$ was dissolved into 50 mL ethanol, respectively. At room temperature, above-prepared solutions were mixed rapidly and stirred vigorously for 24 h. 3 mmol $Fe(NO)_3·9H_2O$ was then added. The mixture was kept stirring for another 12 h at room temperature. The mixed liquid was then centrifuged at 6000 rpm for 10 min. The precipitate was washed three times with ethanol and was dried under vacuum at 60°C. The bimetallic polymer (denoted as Fe/Zn-ZIFs@$ZnCO_3$) of precursor **1** was acquired.

3. Preparation process of precursor 2

For precursor **2**, in a typical process, 5 g of dicyandiamide (DICY), 0.5 g of PEG 2000 and 2 mL of phytic acid (PA) were added into 40 mL of distilled water. Then the mixed solution was stirred at 60°C for 30 min and dried at 80°C.

4. Material characterization

Laboratory powder X-ray diffraction patterns were collected for the samples on a Rigaku Ultima IV X-ray diffractometer with Cu Kα source (40 kV, 40 mA). The morphology and structure of the samples were observed on field-emission scanning electron microscope (FE-SEM, Quant 250FEG) and high-resolution transmission electron microscopy at an acceleration voltage of 200 kV (TEM, JEM-2100F). Micromeritics Belsorp-max analyzer was applied to measure the Brunauer Emmett Teller (BET) surface area and pore size distribution (PSD). X-ray photoelectron spectroscopic (XPS) measurements were conducted on an Axis Ultra instrument from Kratos using monochromatic Al Kα radiation.

5. Electrochemical measurements

All electrochemical measurements were carried out by using a standard three-electrode configuration on a Gamry (RDE710) electrochemical workstation, where the Ag/AgCl (KCl-saturated) electrode and a carbon rod were used as reference and counter electrodes, respectively. To ensure the repeatability of the experiment, the working electrode for each of the four catalysts was prepared by using under uniform condition. The procedure for the preparation of a working electrode was as following: the catalyst powder (5 mg) was dispersed in 0.8 mL of ethyl alcohol with 40 μL of Nafion solution (5 wt %, Sigma-Aldrich) under

sonication to obtain a homogeneous suspension. Then, the catalyst ink (10 μL, 0.30 $mg \cdot cm^{-2}$) was droped on the glass carbon electrode surface. For ORR tests, Cyclic voltammetry (CV) curves were collected in a N_2-saturated or O_2-saturated 0.1 M KOH electrolyte at a scan rate of 50 $mV \cdot s^{-1}$. Additionally, the activity for ORR was also evaluated *via* the RDE method by LSV from 0.2 to -0.8 V in O_2-saturated 0.1 M KOH electrolyte. The ORR stability in O_2-saturated 0.1 M KOH solution was tested by current versus time (i-t) test with a rotating speed of 1600 rpm. The ORR performance of the as-prepared catalysts were make a comparison with the state-of-the-art commercial Pt/C (20 wt%) electrocatalyst (HiSPEC®3000, Alfa Aesar).

Supplementary figures

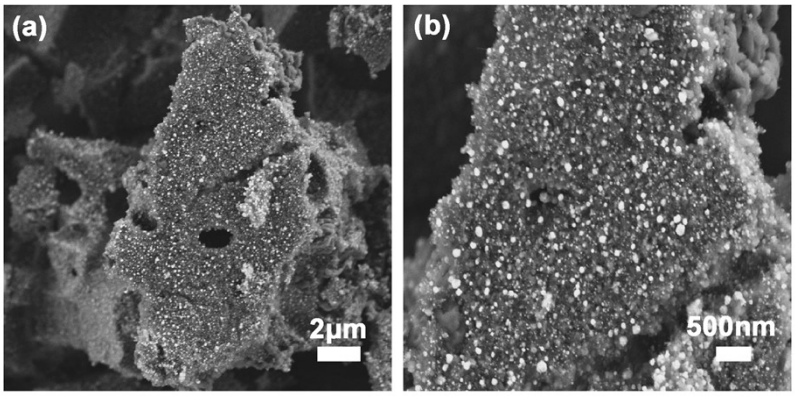

Fig. S1 Representative SEM images of the Fe_3C@NC.

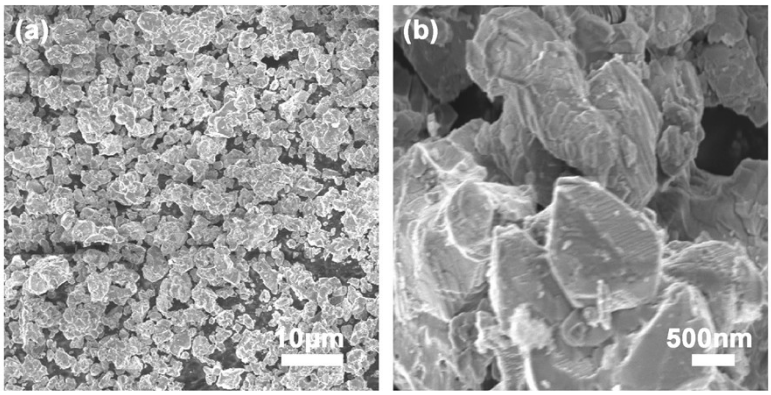

Fig. S2 Representative SEM images of the precursor 1.

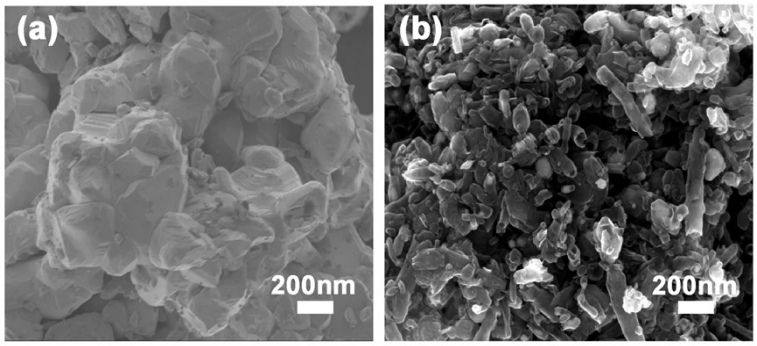

Fig. S3 Representative SEM images of the γ-Fe_2O_3@NPC (a) and the α-Fe_2O_3/γ-Fe_2O_3@NPC (b).

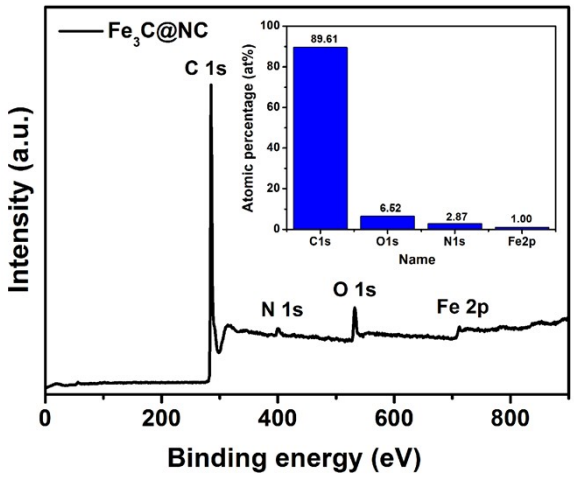

Fig. S4 XPS survey spectrum of Fe_3C@NC.

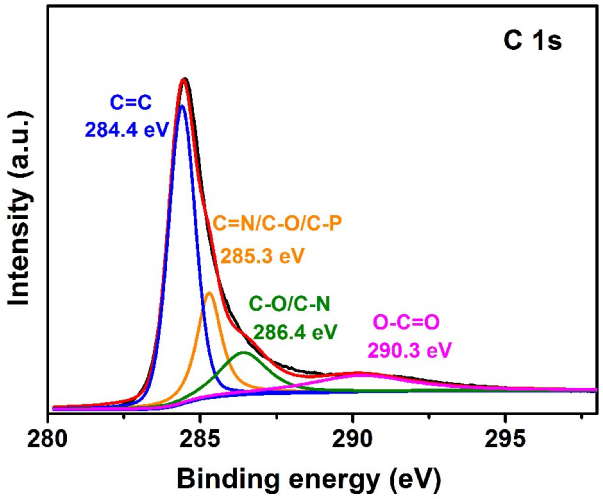

Fig. S5 High-resolution XPS spectrum of C 1s core level for α-Fe_2O_3/Fe@NPC.

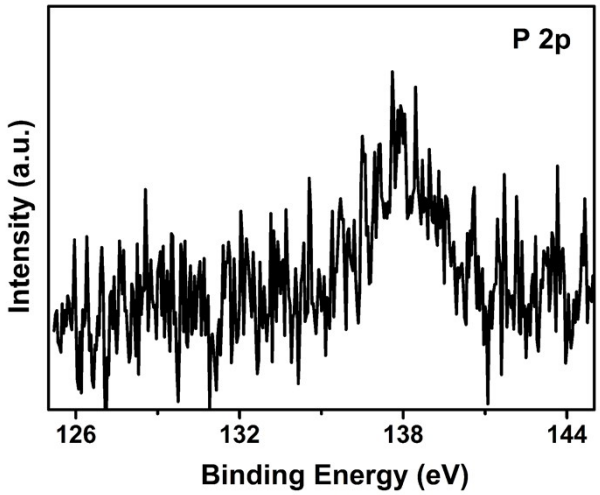

Fig. S6 High-resolution XPS spectrum of P 2p core level for α-Fe_2O_3/Fe@NPC.

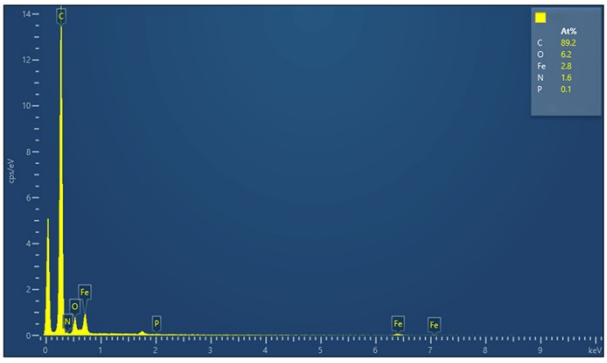

Fig. S7 The corresponding EDS image of α-Fe_2O_3/Fe@NPC.

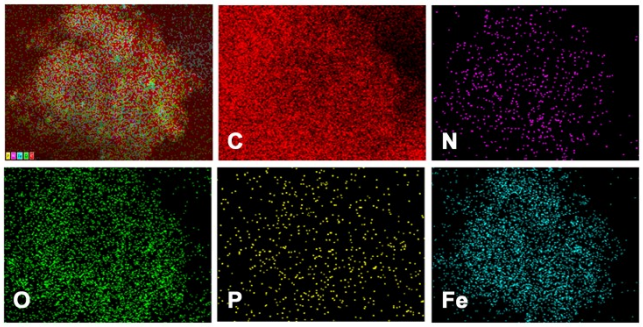

Fig. S8 SEM images of α-Fe_2O_3/Fe@NPC used in the EDS mapping area revealing the elemental distribution of C, N, O, P, and Fe.

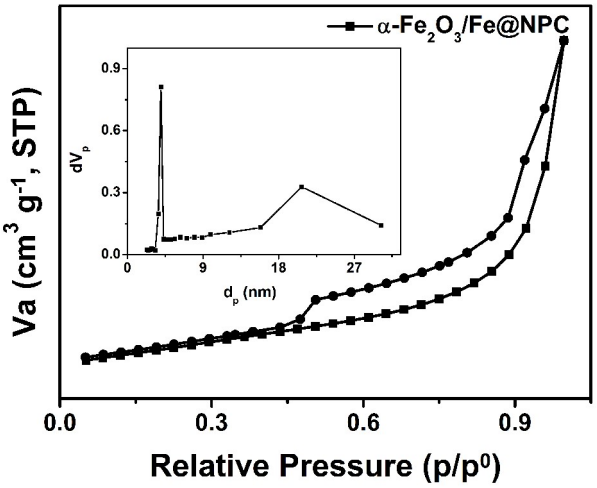

Fig. S9 N_2 adsorption-desorption isotherm of α-Fe_2O_3/Fe@NPC.

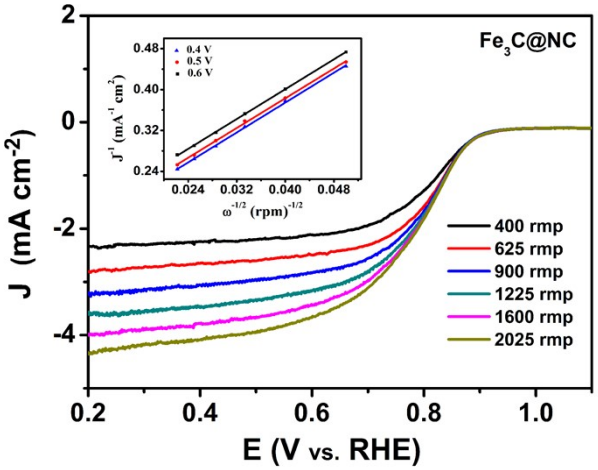

Fig. S10 LSV curves of Fe_3C@NC catalyst in O_2-saturated 0.1 M KOH, respectively. (Inset: K–L plots of Fe_3C@NC at various potentials.)

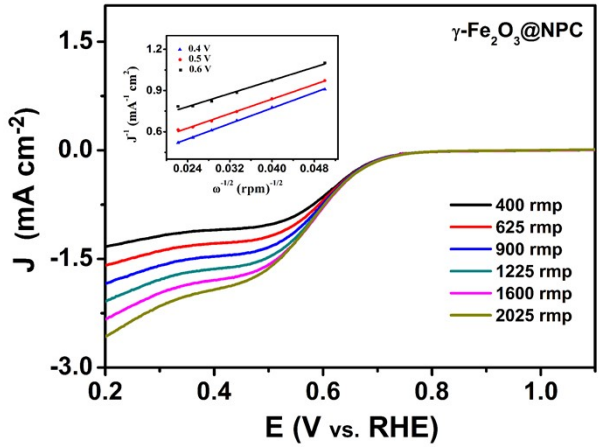

Fig. S11 LSV curves of γ-Fe_2O_3@NPC catalyst in O_2-saturated 0.1 M KOH, respectively. (Inset: K–L plots of γ-Fe_2O_3@NPC at various potentials.)

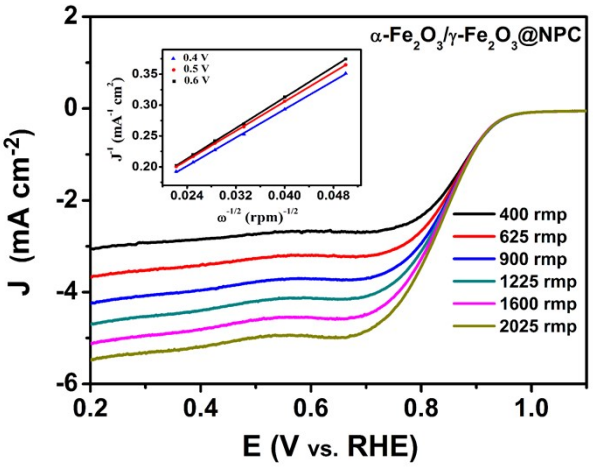

Fig. S12 LSV curves of α-Fe_2O_3/γ-Fe_2O_3@NPC catalyst in O_2-saturated 0.1 M KOH, respectively. (Inset: K–L plots of α-Fe_2O_3/γ-Fe_2O_3@NPC at various potentials.)

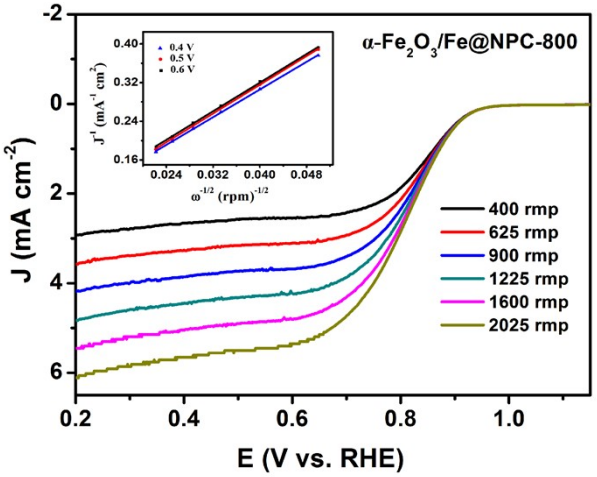

Fig. S13 LSV curves of α-Fe_2O_3/Fe@NPC-800 in O_2-saturated 0.1 M KOH, respectively. (Inset: K–L plots of α-Fe_2O_3/Fe@NPC-800 at various potentials.)

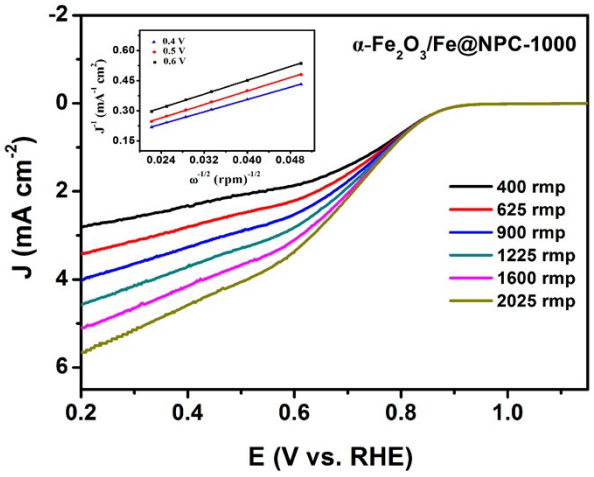

Fig. S14 LSV curves of α-Fe_2O_3/Fe@NPC-1000 in O_2-saturated 0.1 M KOH, respectively. (Inset: K–L plots of α-Fe_2O_3/Fe@NPC-1000 at various potentials.)

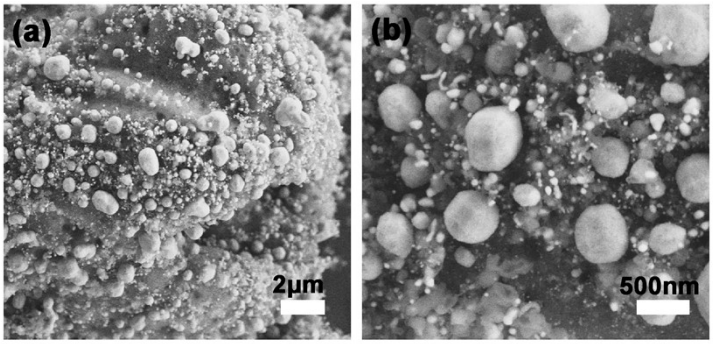

Fig. S15 Representative SEM images of the α-Fe_2O_3/Fe@NPC-800.

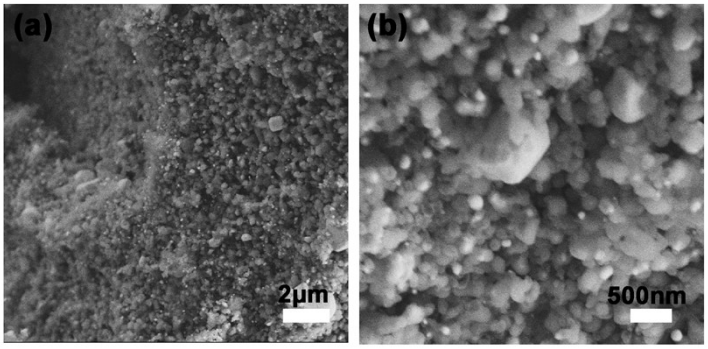

Fig. S16 Representative SEM images of the α-Fe_2O_3/Fe@NPC-1000.

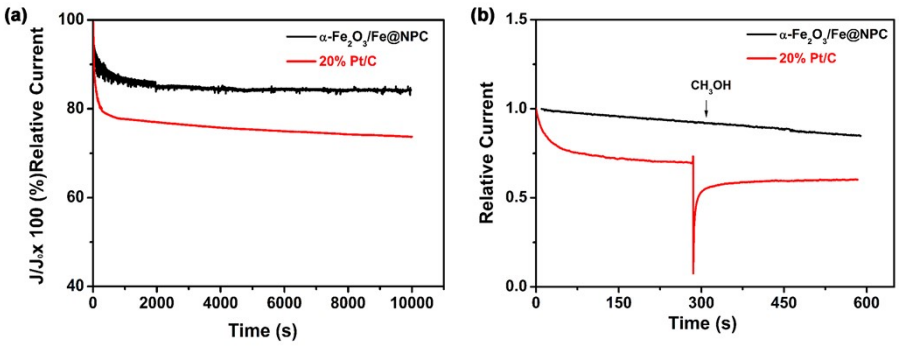

Fig. S17 (a) Amperometric i–t curves of α-Fe_2O_3/Fe@NPC and 20 wt% Pt/C and (b) upon the addition of 3 M methanol in O_2-saturated 0.1 M KOH solution with the rotation speed of 1600 rpm.

Table S1 Levels of C, N, O, P, and Fe of the Fe_3C@NC, γ-Fe_2O_3@NPC, α-Fe_2O_3/Fe@NPC, and α-Fe_2O_3/γ-Fe_2O_3@NPC, respectively.

Sample	Atomic percentage (at%)				
	C	N	O	P	Fe
Fe_3C@NC	89.61	2.87	6.52	0	1.00
γ-Fe_2O_3@NPC	89.83	5.74	3.43	0.12	0.88
α-Fe_2O_3/Fe@NPC	90	5.16	4.41	0.14	0.31
α-Fe_2O_3/γ-Fe_2O_3@NPC	88.98	3.75	5.68	0.04	0.10

Table S2 Atomic percentage of different Fe, N, and O species obtained by XPS spectroscopy.

Sample	Atomic percentage (at%)		
	Fe^0	Fe^{3+}	Fe_2O_3
γ-Fe_2O_3@NPC	21.3	47.3	31.3
α-Fe_2O_3/Fe@NPC	19.4	54.6	26.0
α-Fe_2O_3/γ-Fe_2O_3@NPC	0	70.4	29.6

Sample	Atomic percentage (at%)			
	Pyridinic N	Pyrrolic N	Graphitic N	Quaternary N^+-O^-
γ-Fe_2O_3@NPC	25.2	16.9	36.7	21.2
α-Fe_2O_3/Fe@NPC	29.3	18.6	30.1	21.2
α-Fe_2O_3/γ-Fe_2O_3@NPC	30.7	21.6	33.5	14.2

Sample	Atomic percentage (at%)		
	C=O/P=O	C-O-P	O-H
γ-Fe_2O_3@NPC	44.0	34.5	21.5
α-Fe_2O_3/Fe@NPC	73.1	16.6	10.3
α-Fe_2O_3/γ-Fe_2O_3@NPC	42.9	39.1	18.0

Table S3. The ORR performance of the Fe_3C@NC, γ-Fe_2O_3@NPC, α-Fe_2O_3/Fe@NPC, α-Fe_2O_3/Fe@NPC-800, α-Fe_2O_3/Fe@NPC-1000, α-Fe_2O_3/γ-Fe_2O_3@NPC, and 20 wt% Pt/C in alkaline media at 1600 rpm, respectively.

Sample	E_{onset} (V)	$E_{1/2}$ (V)	J_L (mA cm^{-2})	*n*
Fe_3C@NC	0.93	0.84	4.01	2.96
γ-Fe_2O_3@NPC	0.75	0.59	2.37	1.62
α-Fe_2O_3/Fe@NPC	1.01	0.88	5.06	3.60
α-Fe_2O_3/Fe@NPC-800	0.97	082	5.45	2.95
α-Fe_2O_3/Fe@NPC-1000	0.93	0.77	5.05	2.64
α-Fe_2O_3/γ-Fe_2O_3@NPC	0.97	0.86	5.13	3.62
20 wt% Pt/C	0.96	0.86	5.61	4.00

Table S4. Comparison of the ORR performance for α-Fe_2O_3/Fe@NPC catalyst at 1600 rpm in 0.1 M KOH.

Catalyst	$E_{1/2}$ (V)	J_L (mA cm^{-2})	E_{onset} (V)	Tafel slope (mV dec^{-1})	*n*	Reference
α-Fe_2O_3/Fe@NPC	0.88	5.06	1.01		3.60	This work
α-Fe_2O_3/N-CNTs	0.80	3.1	1.16	90	3.37	*Sci. China Mater.*,2015 [1]
FNTAs	0.79	5.40	0.97	91.0	3.92	*RSC Adv.*, 2016 [2]
α-Fe_2O_3@N-C	0.83	5.67	0.80	115.9	3.46-3.79	*Int. J. Hydrog. Energy.*,2017 [3]
Fe-Fe_2O_3@NC	0.72	2.23	0.92	51.0	3.51-3.92	*Electrochim. Acta*,2017 [4]
a-Fe_2O_3/Fe_3O_4/hNCNC	0.838	6.02	1.03	92.6	3.60-3.90	*J. Mater. Chem. A*, 2018 [5]
Fe_2O_3@NC	0.856	6.492	1.004	74.5	3.976	*Catal. Sci. Technol.*, 2019 [6]
Fe_2O_3@NC&bio-C	0.85	6.0	0.96		3.94	*J. Energy Chem.*,2020 [7]
FeN_x/Fe_2O_3-CNFs	0.81	6.0	0.95		4.0	*J. Mater. Chem. A*, 2020 [8]
γ-Fe_2O_3@CNFs	0.905	4.8	0.915	63.3	4.0	*Chem. Eng.J.*,2021 [9]
Fe_2O_3/G	0.804	6.45	0.92	89.96	3.98-4.0	*New J. Chem.*, 2021 [10]
Fe–CNSs–N	0.835	5.17	0.948	70.6	3.85	*J. Mater. Chem. A*, 2021 [11]
α-Fe_2O_3/A-C_3N_4	0.81	5.2	0.82		3.7	*J Mater Sci*,2022 [12]

Notes and references

1 Sun, M.; Zhang, G.; Liu, H.J.; Liu, Y.; Li, J.H. α-and γ-Fe_2O_3 nanoparticle/nitrogen doped carbon nanotube catalysts for high-performance oxygen reduction reaction. *Sci China Mater* , **2015**, 58, 683–692.

2 Xue, Y.D.; Jin, W.; Du, H.; Wang, S.N.; Zheng, S.L.; Zhang, Y. Tuning α-Fe_2O_3 nanotube arrays for the oxygen reduction reaction in alkaline media. *RSC Adv.*, **2016**, 6, 41878.

3 Fu, Y.; Wang, J.; Yu, H.Y.; Li, X.W.; Wang, H.B.; Tian, J.H.; Yang, R.Z. Enhanced electrocatalytic performances of α-Fe_2O_3 pseudo-nanocubes for oxygen reduction reaction in alkaline solution with conductive coating. *Int. J. Hydrog. Energy.*,**2017**, 42, 20711–20719.

4 Wang, H.; Chen, X.C.; Yin, F.X.; Chen, T.Y.; He, X.B. Metal-organic gel-derived Fe-Fe_2O_3@nitrogen-doped-carbon nanoparticles anchored on nitrogen-doped carbon nanotubes as a highly effective catalyst for oxygen reduction reaction. *Electrochim. Acta*, **2017**, 232, 114–122.

5 Fan, H.; Mao, K.; Liu, M.; Zhou, O.; Zhao, J.; Sun, T.; Jiang, Y.F.; Du, X.; Zhang, X.L.; Wu, Q.S.; Che, R.C. Tailoring the nano heterointerface of hematite/magnetite on hierarchical nitrogen-doped carbon nanocages for superb oxygen reduction. *J. Mater. Chem. A*, **2018**, 6, 21313.

6 Xiao, Z.R.; Shen, G.Q.; Hou, F.; Zhang, R.R.; Li, Y.T.; Yuan, G.; Pan, L.; Zou, J.J.; Wang, L.; Zhang, X.W.; Li, G.Z. Highly dispersed γ-Fe_2O_3 embedded in nitrogen doped carbon for the efficient oxygen reduction reaction. *Catal. Sci. Technol.,* **2019**, 9, 4581.

7 Yan, W. Wu, Y.l.; Chen, Y.L.; Liu, Q.; Wang, K.; Cao, N.; D, F.N. Facile preparation of N-doped corncob-derived carbon nanofifiber efficiently encapsulating Fe_2O_3 nanocrystals towards high ORR electrocatalytic activity. *J. Energy Chem*., **2020**, 44, 121–130.

8 Yu, Q.; Lian, S.T.; Li, J.T.; Yu, R.H.; Xi, S.B.; Wu, J.S.; Zhao, D.Y.; Mai, L.Q.; Zhou, L. FeNx and g-Fe_2O_3 co-functionalized hollow graphitic carbon nanofifibers for efficient oxygen reduction in an alkaline medium. *J. Mater. Chem. A,* **2020**, 8, 6076.

9 Yao, Z.H.; Li, Y.T.; Chen, D.S.; Zhang, Y.W.; Bao, X.H.; Wang, J.; Zhong, Q. *γ*-Fe_2O_3 clusters embedded in 1D porous N-doped carbon matrix as pH-universal electrocatalyst for enhanced oxygen reduction reaction. *Chem. Eng.J.,***2021**, 415, 129033.

10 Haridas, V.; Yaakob, Z.; Sugunan, S.; Narayanan, B. Novel cost-effective synthesis of non-doped turbostratic graphene from a graphite intercalation compound: development of a durable and stable electrocatalyst for the oxygen reduction reaction. *New J. Chem.*, **2021**, 45, 18669.

11 Wang, Y.L.; Gan, R.H.; Liu, H.; Dirican, M.; Wei, C.B.; Ma, C.; Shi, J.L. Zhang, X.W. Fe_3O_4/Fe_2O_3/Fe nanoparticles anchored on N-doped hierarchically porous carbon nanospheres as high-efficiency ORR electrocatalysts for rechargeable Zn-air batteries. *J. Mater. Chem. A*, **2021**, 9, 2764–2774.

12 Chen, F.; Yao, C.C.; Qian, J.C.; Fan, J.J.; Chen, X.W.; Wu, W.J.; Xu, L.; Liu, Q.Q.; Li, W.F. α-Fe_2O_3/alkalinized C_3N_4 heterostructure as efficient electrocatalyst for oxygen reduction reaction. *J Mater Sci*, **2022**, 57, 2012–2020.